Accepted Manuscript

Functional resilience of PSII, vertical distribution and ecosystem-level estimates of subsurface microphytobenthos in estuarine tidal flats

Silja Frankenbach, Andreina A. Azevedo, Vanessa Reis, Diana Dias, Leandro Vaz, João M. Dias, João Serôdio

PII: S0278-4343(19)30109-8

DOI: https://doi.org/10.1016/j.csr.2019.05.018

Reference: CSR 3930

To appear in: *Continental Shelf Research*

Received Date: 21 February 2019

Revised Date: 24 April 2019

Accepted Date: 30 May 2019

Please cite this article as: Frankenbach, S., Azevedo, A.A., Reis, V., Dias, D., Vaz, L., Dias, Joã.M., Serôdio, Joã., Functional resilience of PSII, vertical distribution and ecosystem-level estimates of subsurface microphytobenthos in estuarine tidal flats, *Continental Shelf Research* (2019), doi: https://doi.org/10.1016/j.csr.2019.05.018.

Functional resilience of PSII, vertical distribution and ecosystem-level estimates of subsurface microphytobenthos in estuarine tidal flats

Silja Frankenbach[a,*], Andreina A. Azevedo[a], Vanessa Reis[b], Diana Dias[b], Leandro Vaz[b], João M. Dias[b], João Serôdio[a]

[a] Departamento de Biologia and CESAM – Centro de Estudos do Ambiente e do Mar, Universidade de Aveiro, Campus de Santiago, 3810-193 Aveiro, Portugal

[b] Departamento de Física and CESAM – Centro de Estudos do Ambiente e do Mar, Universidade de Aveiro, Campus de Santiago, 3810-193 Aveiro, Portugal

Corresponding author:

e-mail: s.frankenbach@ua.pt

tel. +351 234370968, fax +351 234372587

Abstract

Most studies on sediment-inhabiting microphytobenthos are based on the biomass present on the surface layers of intertidal flats. However, large amounts of microalgal biomass are known to exist below the surface. This study tested the role of subsurface microalgal biomass as a potential source of photosynthetically active cells for the biofilm on the surface. The resilience of buried cells was evaluated by exposing samples from various depths to surface conditions and investigating the recovery of photosynthetic activity. Additionally, vertical migration by subsurface epipelic diatoms was followed at sub-millimeter scales to evaluate its role for transporting cells to the vicinity of the sediment surface. Finally the relative importance of subsurface microalgal biomass was assessed by estimating the proportion of subsurface:surface biomass for different types of sediments from the Ria de Aveiro. Vertical profiles of chlorophyll *a*, 10 cm-deep, were measured on samples from three intertidal sites, representative of the range of sediment characteristics found in this estuary. The ratio of total biomass to surface biomass ('subsurface biomass fraction') based on total biomass (0-10 cm depth interval; $C_{sub,total}$) and on viable biomass (between the surface and the maximum depth with significant photosynthetic recovery; $C_{sub,viable}$). The experiments showed that buried cells were able to recover photosynthetic activity within 1.5 to 3 hours of light exposure, with the rate of recovery being dependent on depth and type of sediment. Furthermore, subsurface vertical migration was found to enable motile cells to reach the surface from layers deeper than 1 mm within a low tide period. Overall, the results showed that surface biomass (0-0.5 cm) only accounted for one fifth to one third of the total biomass present between the surface and 10 cm, and that the amount of subsurface viable biomass reached 2-3 times the biomass present at the surface.

Applying the estimates of $C_{sub,total}$ and $C_{sub,viable}$ to the whole intertidal area of the Ria de Aveiro, spatially-weighted averages for subsurface biomass fractions were found to reach 3.8 and 2.1 respectively.

Key words: burial, diatoms, epipelic, epipsammic, microphytobenthos, resilience, subsurface, vertical migration

Highlights

- buried microphytobenthos cells can recover photosynthetic activity within 3 hours
- rates of recovery of photosynthetic activity varied with depth and sediment type
- subsurface vertical migration allows cells buried 1 mm deep to reach the surface
- subsurface biomass (0-10 cm) represents 3-5 times the amount at the surface (0-0.5cm)

1. Introduction

Microphytobenthos (MPB) comprises the communities of photoautotrophic eukaryotic algae and cyanobacteria living in intertidal and well-lit subtidal sediments (Underwood and Kromkamp, 1999). Diatoms, a highly diverse group that contributes about 20% to the global primary production and about 40% of the total marine primary productivity (Cahoon, 1999; Field, 1998; Sarthou et al., 2005; Tréguer et al., 2018) usually dominate these communities. Diatoms also serve as basis for many marine food webs (Armbrust, 2009), constitute a key carbon source for heterotrophs (Middelburg et al., 2000), and contribute to sediment stabilization through the production of extracellular polymeric substances (EPS) (Cahoon, 1999). Not surprisingly, MPB has been the object of intense research, mostly centered on the seasonal dynamics of biomass and estimation of annual productivity budgets (Benyoucef et al., 2014; Brito et al., 2009; Du et al., 2010b; Koh et al., 2007; Moerdijk-Poortvliet et al., 2018; Pinckney and Zingmark, 1993; Stanley and Howard, 2013).

Most studies have focused on the microalgal biomass within the photic zone, where light penetrates enough to support photosynthetic activity and primary productivity (Herlory et al., 2004; Kelly et al., 2001; MacIntyre and Cullen, 1995; Serôdio et al., 2001). However, large amounts of microalgal biomass can be found well below the surface of the sediment (Brotas and Serôdio, 1995; De Jonge and Colijn, 1994; Fenchel and Straarup, 1971; Mundree et al., 2003; Steele and Baird, 1968). This is especially significant considering that the photic zone in sediments is very thin. It spans from the surface to a few millimeters in sandy sediments, to only fractions of a millimeter, in muddy sediments (Cartaxana et al., 2011; Herlory et al., 2004; Kelly et al., 2001).

MPB cells are continuously buried below the surface due to bioturbation and resuspension/deposition events caused by waves and currents during high tide (de Jonge and van Beusekom, 1995; Kingston, 1999; Plecha et al., 2014; Ubertini et al., 2015). Conversely, buried cells can return to the surface, being passively transported either during bioturbation and resuspension events, or due to the reworking or removal of upper layers of sediment by grazers like snails or fish (Almeida et al., 1993; Hagerthey et al., 2002), exposing cells in a newly created surface. While these processes occur in all types of sediments, in the case of muddy sediments the resurfacing of cells may be enhanced by vertical cell migration. In contrast with sandy sediments, where the diatom communities are mainly formed by non-motile lifeforms (epipsammic) living attached to the large sediment particles, in muddy sediments the MPB is dominated by raphid pennate diatoms (epipelic), able to actively move between the fine sediment particles (Admiraal, 1984; Cahoon et al., 1995).

Although most studies have focused on the effect of vertical migration on the biomass present at the surface or in the photic zone (Easley et al., 2005; Round and Palmer, 1966; Serôdio et al., 2001), motile diatoms may undertake vertical migratory movements at sedimentary depths below the illuminated layers (Frankenbach et al., 2014; Pinckney et al., 1994). However, subsurface vertical migration has been poorly studied and its potential importance for reaching newly-created surface layers is unknown.

Subsurface biomass has been hypothesized to represent a source of photosynthetically competent cells capable of ‘re-inoculating’ the depleted surface, and thus allowing the attenuation of in the biomass the photic zone and biofilm productivity (Delgado et al., 1991; Easley et al., 2005). This requires that the buried diatoms survive prolonged periods in continuous darkness, and regain their photosynthetic activity

quickly (faster than growth of remaining cells) following exposure to surface conditions. In order to contribute to this process, buried epipelic species need to retain their capability to migrate vertically to reach the photic zone.

This study tested the importance of subsurface microalgal biomass as a potential source of photosynthetically active cells for surface MPB biofilms. This was pursued by addressing the following objectives in the described ways:

(i) to investigate if buried cells can regain photosynthetic activity in a short time if exposed to surface conditions; to determine until which depth can cells recover their photosynthetic competence. These questions were addressed by following the recovery of photosynthetic activity of subsurface MPB samples, from various depths, following resurfacing and exposure to ambient light.

(ii) in the case of epipelic MPB communities, to test if vertical migration occurring below the surface are capable of transporting cells to the vicinity of the sediment surface. This was studied by measuring vertical migration at sub-millimeter vertical scales, using a recently-developed method for obtaining thin sediment sections.

(iii) to estimate how much microalgal biomass is present below the surface, relative to surface levels, and to determine if the proportion subsurface:surface biomass varies with sediment type. These questions were addressed by measuring vertical profiles of MPB biomass for various sediment types and quantifying the subsurface MPB biomass, distinguishing ‘total’ biomass (down to 10 cm deep) and ‘viable’ (down to the depth determined in (i)).

(iv) to estimate the amount of subsurface MPB biomass present at the ecosystem level. This was estimated considering the proportion of subsurface biomass for different types of sediments and associated MPB communities, and the spatial distribution of

sediment types throughout the intertidal areas of one estuarine ecosystem, the Ria de Aveiro (Portugal).

2. Material and methods

2.1. Sampling sites

The Ria de Aveiro is a mesotidal coastal lagoon on the northwest coast of Portugal (40º38'N - 08º45'W) (Tomás et al., 2014). Detailed characterization of physical, geomorphological, and ecological features of the Ria de Aveiro can be found in Bueno-Pardo et al., (2018); Dias et al.,(2003, 1999); Tomás et al., (2014). Sampling was carried out on intertidal sites considered as representative of the overall variability in sediment type. MPB assemblages were collected in two channels of the lagoon: Gafanha da Encarnação (GE; in Canal de Mira, 40°35'18" N, 08°41'06" W), and Vista Alegre (VA; in Canal de Ílhavo, 40°37'12" N, 08°44'54" W). The sampling sites differ in grain size, salinity (Tomás et al., 2014; Vargas et al., 2017), and water retention time (Dias et al., 2003). Sediment granulometry ranged from sand (45.3% particles between 63 µm and 125 µm; 42.7% below 63 µm) at GE, to finemud (97% of the grains smaller the 63 µm) at VA (percentages of dry weight; Serôdio et al., 2007). The MPB communities of the two sites have distinct taxonomic composition and photophysiological characteristics (Frankenbach et al., 2018; Serôdio et al., 2007). To increase the spatial resolution of the estimation of the subsurface biomass at the ecosystem-level, a third sampling site was added. This site is located in the Canal de Ovar, in front of Torreira (TO; 40º35" N,8º,42" W)

165 *2.2. Recovery of photosynthetic activity*

166

167 On three consecutive days in July 2016, 12 sediment cores were collected using
168 2 cm-diameter, 20 cm-long acrylic corers during daytime low tide and taken to the
169 laboratory. There, the cores were sectioned horizontally into 5 mm-thick sections. The
170 sections started at depth 0, 5, 20 and 40 mm (VA) or 0, 20, 45 and 60 mm (GE) below
171 the surface. In the case of GE samples, the depth intervals were adjusted to reach deeper
172 layers because in sandy sediments resuspension and bioturbation are expected to cause
173 sediment mixing down to greater depths. Each section was cut with a separate blade,
174 forming the base of a circular plastic ring 5-mm thick, avoiding cross contact and
175 transfer of sediments between sections. Three replicated cores for each sampling site
176 were used.

177 Shortly after sectioning, the undisturbed samples were exposed to constant low
178 white light (50 µmol photons m^{-2} s^{-1}), provided by a LCD digital projector (EMP-1715;
179 Epson, Suwa, Japan) for six hours, simulating the exposure to surface conditions
180 following resurfacing. This light intensity is high enough to induce photosynthetic
181 activity and promote upward migration of MPB, but low enough to avoid damaging
182 light stress (Serôdio et al. 2006, Laviale et al. 2016). During this period, the
183 photosynthetic activity of the cells in the newly exposed sediment surfaces was
184 monitored by measuring Φ_{PSII}, the effective quantum yield of photosystem II (PSII),
185 every 30 min. At the end of this period, the samples were used to quantify the Chl *a* and
186 water content, as well as for determination of taxonomic composition (see below). Φ_{PSII}
187 was measured using a Pulse Amplitude Modulated (PAM) fluorometer (WATER-
188 EDDF-Universal PAM, Gademann Instruments; (Serôdio, 2004), using a 6 mm-
189 diameter optical fiber to deliver measuring light and saturating pulses (peaking at 450

nm) and to capture the emitted fluorescence. Φ_{PSII} was determined by measuring steady state (F_s) and maximum (F_m') fluorescence levels ($\Phi_{PSII} = (F_m' - F_s)/F_m'$) (Genty et al. 1989). Three independent saturating pulses were applied to each sample by positioning the optical fiber at different non-overlapping areas (1 mm from the surface, 45°). The average Φ_{PSII} for each sample and time point was used in subsequent calculations. The variation of Φ_{PSII} over time during light exposure was described by a rate constant of Φ_{PSII} recovery, k_t (min^{-1}), estimated by fitting the following model:

$$\Phi_{PSII}(t) = \Phi_{PSII}(ss) + [\Phi_{PSII}(t_0) - \Phi_{PSII}(ss)]e^{-k_t t} \quad (1)$$

where $\Phi_{PSII}(t_0)$ and $\Phi_{PSII}(ss)$ are the PSII effective quantum yields at the beginning of the exposure (t_0) and after reaching a steady state.

In order to verify the source of the observed fluorescence signal at each depth, three additional cores were sliced and exposed to comparable light conditions (intensity and duration) using a second LCD digital projector (EB-X14; Seiko, Japan). The cells were harvested at the end of the experiment by carefully scraping off the uppermost surface layer. Samples were then fixed in Lugol's solution (concentrated, 5% Iodine, AppliChem GmbH, Germany) and stored at 4 °C. The abundance of the major photoautotroph taxonomic groups was examined using a Nageotte counting chamber (Marienfeld-Superior, Germany). Observed cells were grouped into three categories; diatoms, cyanobacteria, and euglenoids. Cells that were not possible to identify were grouped as 'others' to avoid overestimation of abundance for other groups.

2.3. Subsurface vertical migration

To test the capacity of cells displaced to layers below the surface to migrate vertically, homogenized slurries were used to simulate a disturbance event such as bioturbation or resuspension/deposition. During low tide, sediment was collected from the top 1 cm using a spatula and deposited in a tray overnight in the laboratory. The following day, at the time coinciding with the beginning of low tide exposure in the field, the samples were thoroughly mixed using a spatula, and the homogenized slurries were poured into 24-wellplates as described in Frankenbach and Serôdio (2017). Immediately after the sample preparation, a first sampling was carried out by collecting surface samples of different thickness (of 0.1, 0.25, 0.5 and 1.0 mm-thick) using the cryo-sampling technique "crème brûlée" (Laviale et al., 2015). This procedure was repeated during the subjective low tide period, once at the time of the low peak tide in the field, and 90 min before and 90 min after that time. The sediment samples were immediately transferred into pre-weighted Eppendorf-caps and shock frozen in liquid N_2, and microalgal biomass was later quantified by measuring Chl *a* content. The changes in biomass at each depth interval allowed to follow the variation of biomass over time and along vertical profiles, with sub-millimeter resolution. Biomass present in each depth interval below the surface (0.1-0.25, 0.25-0.5 and 0.5-1.0 mm) was estimated by subtracting the Chl *a* content of a sample of a certain thickness from the Chl *a* content of the sample of thickness immediately higher. Three replicates were obtained for each time and depth interval. This experiment was carried out exclusively for samples from VA, as the communities from GE are dominated by epipsammic forms, and therefore not expected to show significant motility.

2.4. Vertical distribution of subsurface biomass

Vertical profiles of Chl *a* were measured in samples collected from the three sampling sites described above. Sediment cores (36 mm diameter, 20 cm long) were collected during low tide. The cores were sectioned into 5 mm-thick sections in the uppermost 20 mm, and 20 mm-thick from 20 mm down to 100 mm below the surface. Chl *a* depth profiles were quantitatively described by fitting a simple negative exponential model, based on the one proposed by Brotas and Serôdio (1995). The model used in the present study contains a new parameter, C_d, representing the minimum background level approached by the Chl *a* content as depth increases:

$$C(z) = C_0 e^{-k_c z} + C_d \quad (2)$$

where C(z) and C_0 are the Chl *a* content at any depth z and at the surface (z = 0), respectively, and k_C represents the rate constant of Chl *a* decay with depth. When fitting the model, the median depth of each sediment section was used as z. The model was used to calculate, for each type of sediment, the ratio of total biomass (including surface and subsurface) to surface biomass:

$$C_{sub,total} = \frac{\int_0^{z_t} C(z)dz}{\int_0^{z_s} C(z)dz} \quad (3)$$

where z_t is the maximum depth where Chl *a* was found (considered here as 10 cm) and z_s is the depth defining the 'surface' layers (here considered 5 mm). This ratio, the 'subsurface biomass fraction' (C_{sub}) allows to estimate the total, depth-integrated MPB biomass from surface biomass measurements (see below). C_{sub} was also calculated based on the 'viable' biomass, defined as the depth-integrated Chl *a* content present

between the surface and the maximum depth at which significant recovery was observed following exposure to surface conditions:

$$C_{sub,viable} = \frac{\int_0^{z_v} C(z)dz}{\int_0^{z_s} C(z)dz} \quad (4)$$

where z_v is the maximum depth where potentially viable cells are present. z_v was determined from the results of the experiments on photosynthetic resilience (see above).

2.5. Ecosystem-level subsurface biomass fraction

The fraction of MPB subsurface biomass was estimated for the whole intertidal area of the Ria de Aveiro, considering the relationship between C_{sub} values and sediment type (granulometry) observed for the sampling sites and the distribution of granulometry throughout the intertidal areas of the estuary. Information on the grain size of the sediments of the Ria de Aveiro was obtained from Costa et al. (2018) and Plecha et al. (2014). The available data is the form of a D_{35} matrix, values that correspond to the size of particles where 35% of all particles have a lower diameter than the announced value. For the three sampling sites, the D_{35} values were 2.9×10^{-4} m (VA), 3.3×10^{-4} m (TO) and 6×10^{-5} m (GE), respectively, meaning that sediments from GE have comparably larger particles (sandy) and VA the finest (muddy). The geographic information system software ArcGIS (ERSI, USA) was used to create a map of the lagoon under different tidal conditions, based on Google Earth´s satellite imagery. Multiple images of different tidal cover situations were used to map the intertidal and subtidal areas of the estuary. For each intertidal area polygon constructed, the

correspondent C_{sub} values were defined according with D_{35} data matrix. The software calculated the areas automatically, after the correct georeferencing.

2.6. Chlorophyll a *quantification*

The samples used for testing recovery of PSII functionality and vertical migration were extracted in 2 mL cold acetone (90%). For Chl *a* vertical profiles samples, the water content of three replicated cores was determined for each depth on additional replicates and the average value was used to calculate the volume of acetone (100%) to be added to achieve a final concentration of 90%. Chl *a* content is given as weight of Chl *a* per dry weight of sediment. The dry weight was determined by drying the samples at 120 ºC for 24 h. In all cases, Chl *a* extraction was made in the dark, 4 ºC for 24 h. Chl *a* concentration was calculated according to Lorenzen (1967). Extracts were centrifuged (10 min, 18000 g, 4 °C). The absorbance of the supernatant was measured at 664 and 750 nm before and after acidification (10 µL, 1 N HCl), using a spectrophotometer (Thermo Spectronic, Rochester, NY, USA).

2.7. Statistical analysis

The Φ_{PSII} values measured at different depths and at the surface were compared by applying a two-tailed Student´s *t*-test.

3. Results

3.1. Recovery of photosynthetic activity

The exposure of buried cells to surface conditions resulted in significant and relatively fast recovery of Φ_{PSII} in both types of sediments. However, the Φ_{PSII} recovery capacity varied markedly with depth and sediment type. In both types of samples, the initial values of Φ_{PSII} decreased with depth. In VA samples, $\Phi_{PSII}(t_0)$ decreased from 0.68 ± 0.03 at the surface to 0.46 ± 0.06 and 0.38 ± 0.02 at the depths of 2.0 and 4.0 cm, respectively (Fig.1a). During light exposure, cells present at the surface showed only a slight increase in Φ_{PSII}, which stabilized at around 0.71 ± 0.02 within the first hour. On samples from deeper layers, light exposure caused substantial increases in Φ_{PSII}, up to 64% (4.0 cm deep, after 3 h) (Fig 1a). After 6 h of light exposure, Φ_{PSII} increased by about 0.4% (0.69 ± 0.007 surface), 8% (0.68 ± 0.021 0.5 cm) and 42% (0.65 ± 0.235; 2.0 cm), 56% (0.59 ± 0.026; 4 cm). For all depths, the steady state values of Φ_{PSII} were significantly lower than the ones at the surface (*t*-test, $P < 0.001$). Plotting the same data as a function of depth highlights how most of the recovery of Φ_{PSII} happened within the first 3 hours (Fig. 1b).

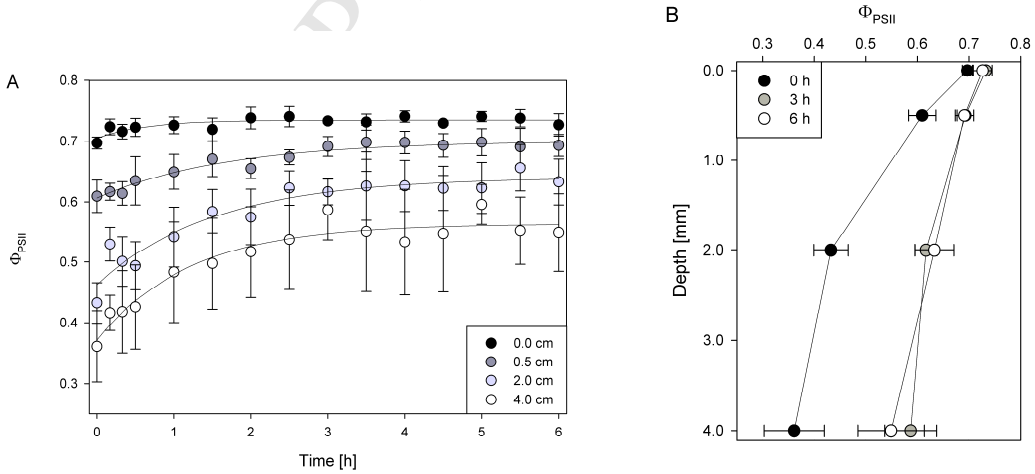

Fig. 1. Recovery of PSII effective quantum yield (Φ_{PSII}) of samples collected at VA following exposure to surface conditions, for different depths. (A) Variation of Φ_{PSII} over time for four different depths. Lines represent the fitting of Eq. (1) to data collected

for each depth. (B) Φ_{PSII} plotted against depths for three time points. Average of three independent measurements. Error bars indicate one standard error.

In contrast with VA samples, $\Phi_{PSII}(t_0)$ of GE samples was generally lower, although the variation with depth was less pronounced. Furthermore, the recovery of photosynthetic activity was essentially limited to the top 2.0 cm. Starting from values of Φ_{PSII} = 0.540 ± 0.028, surface samples showed a small increase to 0.620 ± 0.001, reaching a steady state within the first hour of light exposure. At 2.0 cm, Φ_{PSII} increased 66%, from 0.20 ± 0.05 to 0.43 ± 0.019 in the first 90 min of light exposure, after which no further changes were observed (Fig. 2a). This was comparable to the increase of Φ_{PSII} observed for VA at 4.0 cm after 3 h of light exposure. Samples from deeper layers (4.5 and 6.0 cm) showed only a very small recovery of Φ_{PSII} from about 0.22 ± 0.01 to 0.26 ± 0.02 and 0.22 ± 0.03 to 0.26 ± 0.04 respectively, after 6 h of light exposure. Vertical profiles of Φ_{PSII} highlight how recovery was limited to the top layers, mostly to the layers 2.0 cm deep (Fig. 2b).

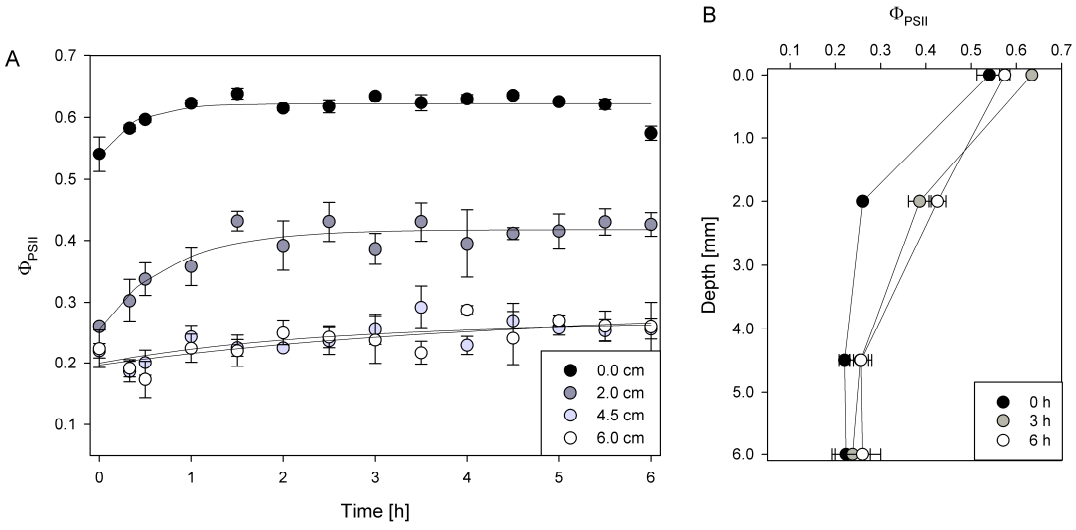

Fig. 2. Recovery of PSII effective quantum yield (Φ_{PSII}) of samples collected at GE following exposure to surface conditions, for different depths. (A) Variation of Φ_{PSII}

over time for four different depths. Lines represent the fitting of Eq. (1) to data collected for each depth. (B) Φ_{PSII} plotted against depths for three time points. Average of three independent measurements. Error bars indicate one standard error.

The different recovery capacity of VA and GE samples is confirmed by the rate constant of Φ_{PSII}, k_t, and its variation with depth (Fig. 3). While for GE, k_t reaches high values (> 1.25 min^{-1} for surface and depth 2.0 cm) and decreases considerably with depth, for VA samples k_t remained below 1.0 min^{-1}, and varied much less with increasing depth.

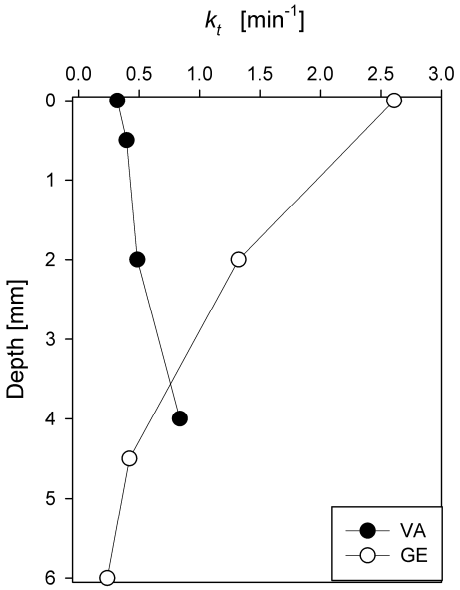

Fig. 3. Variation with depth of the rate constant of Φ_{PSII} recovery (k_t) for samples collected at VA and GE.

The relative distribution of the main taxonomic groups with depth is shown in Fig. 4. Both VA and GE samples showed a clear dominance of diatoms at all depths, with the minimum diatom abundance being observed for GE samples at 6.0-6.5 cm with 72 ± 4.28%. Cyanobacteria were present in almost all samples (the exception GE samples, at 6.0 cm) and euglenoids were observed only in VA samples.

374

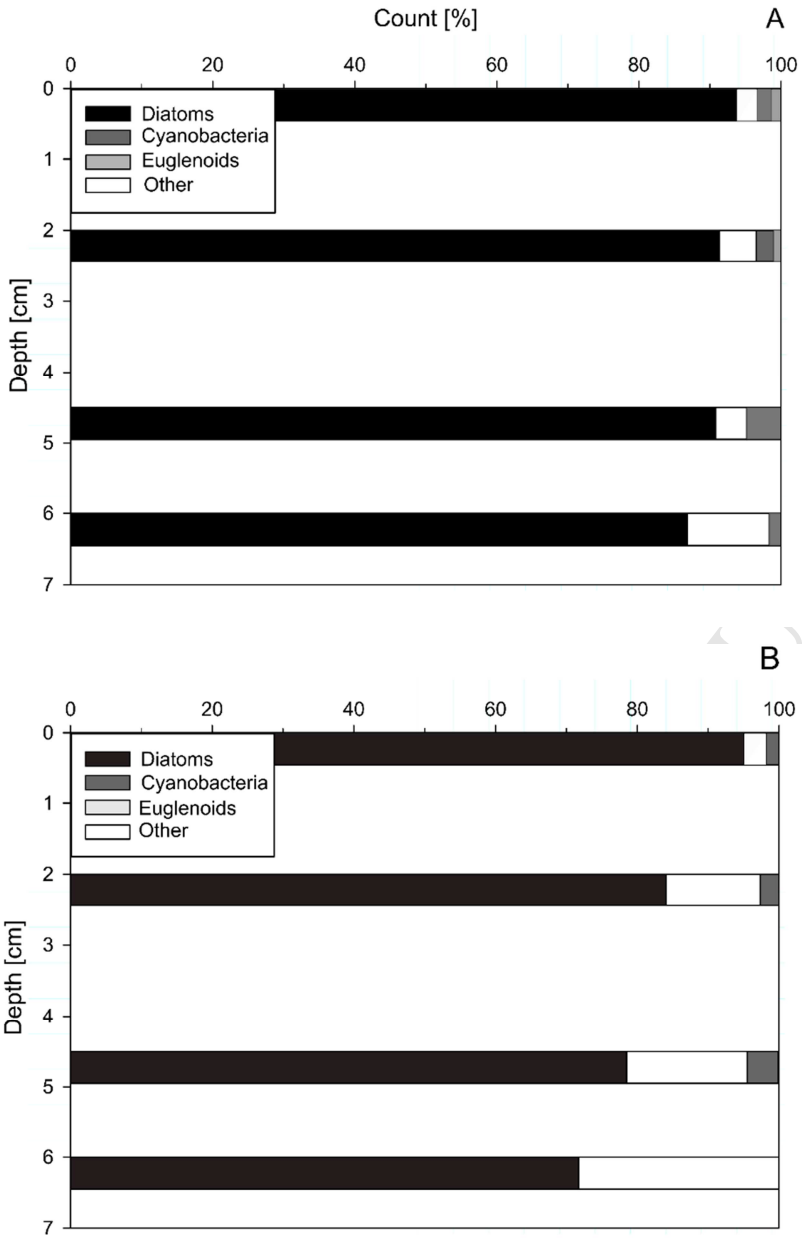

375

376

377 Fig. 4. Variation with depth of the relative abundance of three main taxonomical groups
378 (diatoms, cyanobacteria and euglenoids) in sampling sites VA (A) and GE (B). Cells
379 categorized as 'other' were in most cases unidentified.

380

381

382 *3.2. Subsurface vertical migration*

383

Fig. 5 shows the results of two independent experiments following the variation of sub-millimeter vertical profiles of Chl *a* concentration during a low tide period. In both cases, a clear surface accumulation of microalgal biomass was observed in all sampled depths, but mainly above 0.4 mm. On some occasions, a subsurface maximum was observed, denoting the upward movement of cells toward the surface. Although the experiments started from homogenized slurries, already in the first sampling occasion some cell accumulation towards the surface was observed, indicating that vertical migration towards the surface started immediately after the homogenization of the sediment. Maximum Chl *a* concentrations (308.9 and 275.7 µg mm^{-3}) were reached at the time coinciding with the time of low tide in the field, which was 3 h after the start of the experiment. Thereafter, a downward bulk movement appeared to have started, corresponding to the downward migration anticipating the incoming tide in the field. In both experiments, the total Chl *a* in the uppermost 1 mm increased over time, denoting the accumulation of cells originating from deeper layers due to vertical migration occurring below the surface (Fig. 5).

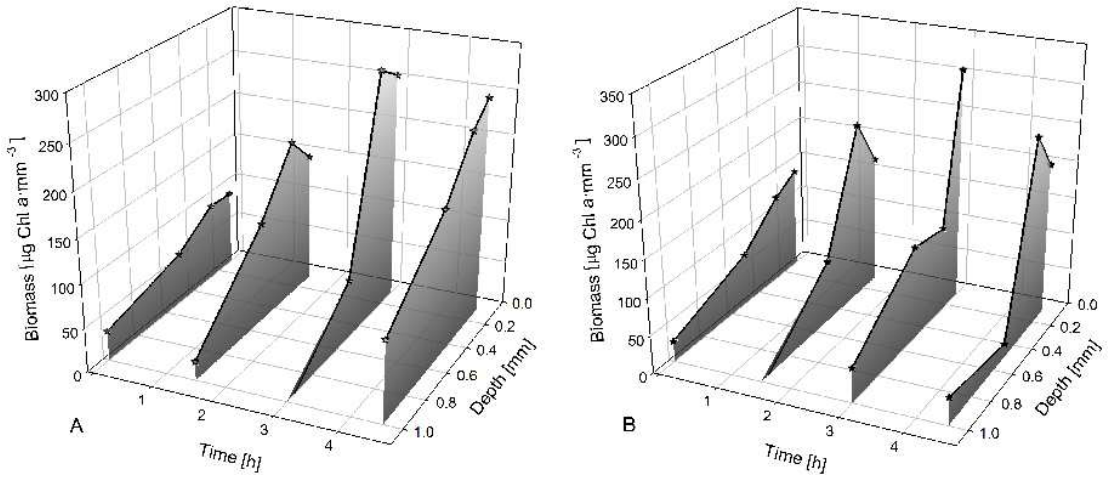

Fig. 5. Variation of sub-millimeter scale Chl *a* vertical profiles over the time course of a diurnal low tide exposure. Panels A and B refer to two independent experiments. Average of three independent samples.

The two experiments differed such that in the latter (Fig. 5B), the total Chl *a* reached a maximum and started to decrease before the end of the measuring period, while in the former (Fig. 5A) it continued to increase throughout the whole sampling period (Fig. 6).

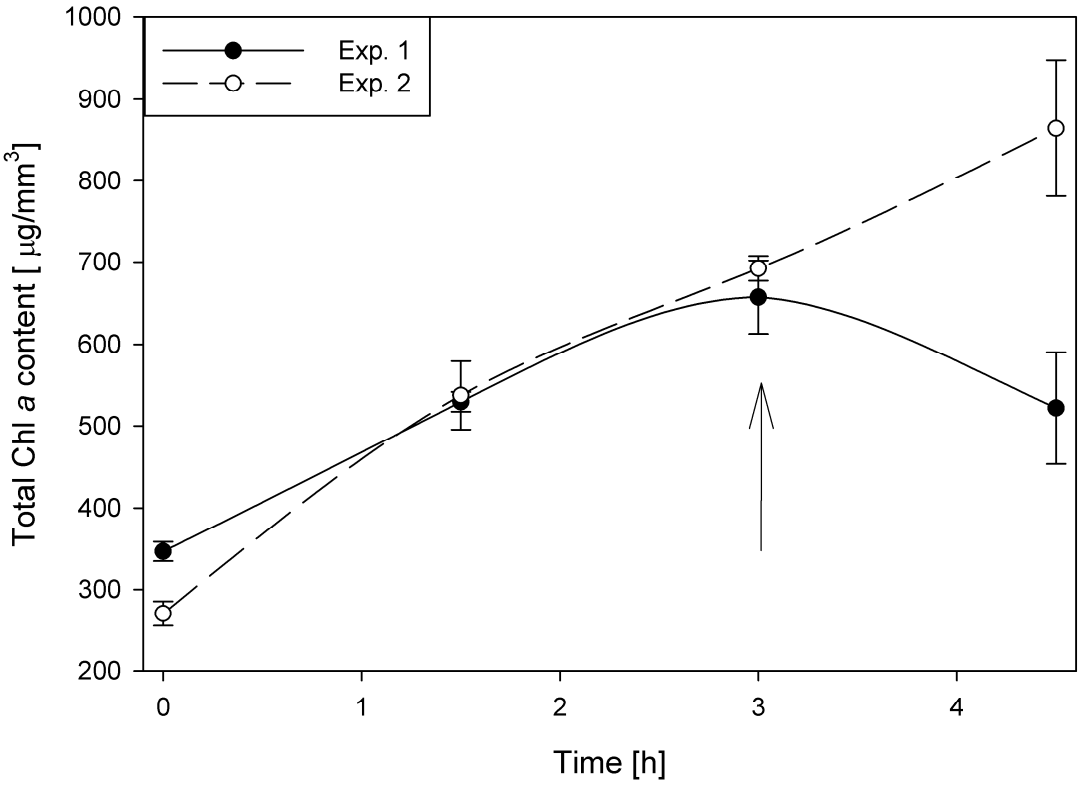

Fig. 6. Depth-integrated Chl *a* content over the time course of a diurnal low tide exposure, during two independent experiments (from data shown in Fig. 5). Arrow indicates the low tide peak at the corresponding sampling side.

3.3. Vertical distribution of MPB biomass

Sediment cores sampled in VA showed the highest Chl *a* content at the surface, averaging 28.4 ± 1.93 µg Chl *a* g^{-1}, which gradually decreased with depth to a minimum of 4.0 ± 0.96 µg Chl *a* g^{-1} at 10 cm (Fig. 7a). The lowest surface Chl *a* content was measured in GE samples, reaching only 5.5 ± 1.58 µg Chl *a* g^{-1}, and decreasing to a minimum of 0.90 ± 0.31µg Chl *a* g^{-1} at the depth of 10 cm (Fig. 7c). Sediment cores sampled in TO showed intermediate values, reaching 15.85 ± 2.22 µg Chl *a* g^{-1} at the surface and minimum values of 4.57 ± 1.58 µg Chl *a* g^{-1} at 10 cm (Fig. 7b). In all cases, the decrease with depth followed a negative exponential-like pattern, which enabled a very good fit of Eq. (2) ($r^2 > 0.96$ in all cases) and estimation of parameters C_0, k_C, and C_d for each type of sediment (Fig. 7). The values of k_C were similar in VA and GE samples (1.11 and 1.26 cm^{-1}, respectively), despite the large difference in Chl *a* content of the two profiles (Fig. 7). The TO samples showed an intermediate Chl *a* content and a much lower rate of decrease (k_C = 0.53 cm^{-1}), indicating a more vertically homogeneous profile. In all cases, the profiles tend to a non-null constant Chl *a* content level (C_d).

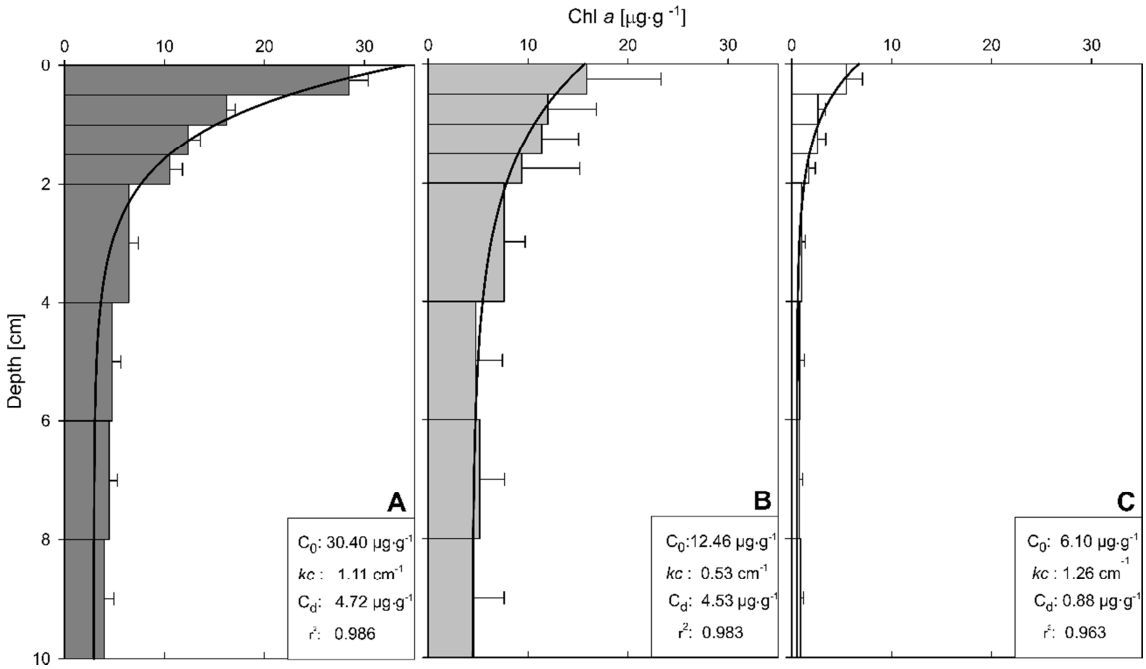

Fig. 7. Depth profiles of Chl *a* content in the three sampling sites VA (A), TO (B) and GE (C). Line represents the fitting of Eq. (2). The estimated values of the parameters of Eq. (2) C_0, k_C, and C_d are shown. Average Chl *a* concentration of nine sediment cores. Error bars indicate one standard error.

Using the estimates of the parameters C_0, k_C, and C_d for each site, the subsurface fraction $C_{sub,total}$ was calculated by applying Eq. (3), resulting in the following values: 4.95 (VA), 5.17 (TO) and 2.96 (GE). These values indicate that the surface MPB biomass (0-5 mm depth range) only accounts for around one fifth to one third of the total MPB biomass present in the sediment (considered down to 10 cm). The subsurface fraction for potentially viable biomass was calculated by applying Eq. (4), and, considering the values for z_v of 3.0 cm (VA) and 2.0 cm (TO, GE), resulted in the following values: 3.14 (VA), 2.30 (TO) and 1.92 (GE). These results indicate that the proportion of subsurface MPB biomass capable of regaining photosynthetic activity after surfacing reaches roughly 2-3 times the biomass present in the top 5 mm.

3.4. Ecosystem-level subsurface biomass fraction

Making use of the known distribution of sediment granulometry and of the C_{sub} values for the sampled sediments, maps of the spatial distribution of the fraction of total and viable subsurface MPB biomass were produced (Fig. 8). These maps allowed classifying the intertidal areas according to the relative amount of subsurface MPB biomass. By calculating the total area of each type of sediment and corresponding C_{sub} values, spatially-weighted averages for subsurface biomass fraction for the entire Ria de Aveiro was estimated: 3.78 for $C_{sub,total}$ and 2.14 for $C_{sub,viable}$.

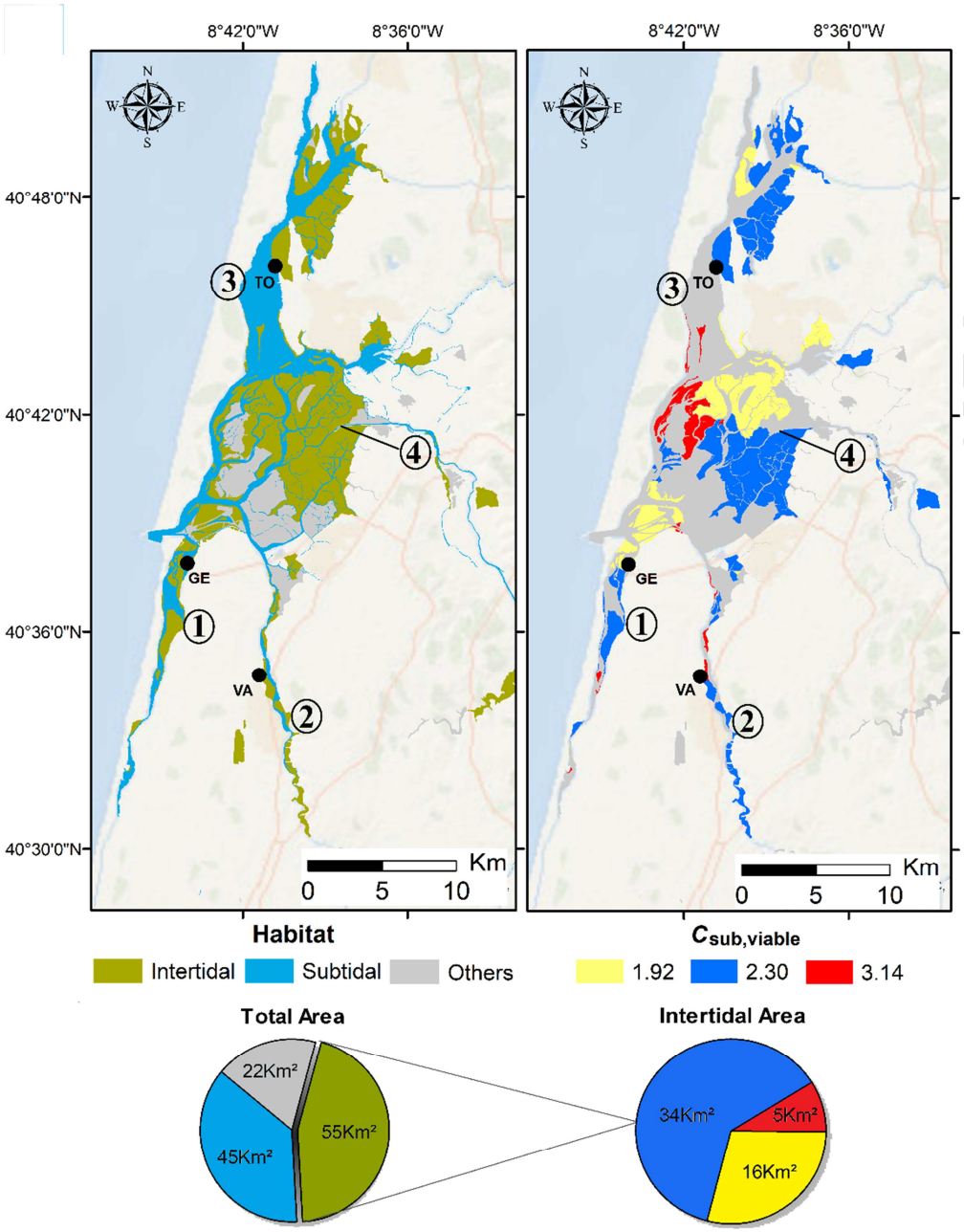

Fig. 8. Classification of the intertidal areas Ria de Aveiro regarding the ratios of total biomass and of total viable biomass to surface biomass ($C_{sub,total}$ and $C_{sub,viable}$, respectively). Values of $C_{sub,total}$ and $C_{sub,viable}$ determined for each intertidal habitat were applied to the total intertidal area. Numbers identify the main channels: Mira Channel (1), Ílhavo Channel (2), São Jacinto Channel (3), Espinheiro Channel (4).

4. Discussion

473

474 *4.1. Photosynthetic resilience*

475

476 This study showed that buried MPB cells s can regain PSII functionality shortly
477 after being exposed to surface conditions, although it varied between the two sediment
478 types. These results expand the findings of Wasmund (1989) on subtidal MPB, which
479 demonstrated that buried microalgae are able to fix CO_2 after exposure to light in one
480 sediment sample. The present study includes, however, photosynthetic recovery kinetics
481 in muddy and sandy sediments inhabiting MPB. Samples from muddy sediments (VA)
482 showed that the capacity to recover was extended to deeper layers than those of the
483 sandy site GE. The capacity to recover was related to the initial physiological status at
484 each depth, as initial ΦPSII levels decreased with depth. Cell viability was seen to
485 decrease with depth in both sampling sites, and cells found in deeper layers can be
486 thought to have spent longer periods away from the surface. The idea that cells from GE
487 spend more time buried may contradict what is expected from the fact that muddy
488 sediments are typically more cohesive than sandier ones. However, it distinct lifeforsm
489 (no motile, epipsammic in sandy, vs motile eipipelic froms in dominated in
490 muddysediemnts) might be part of the explanation. Furthermore, surface biomass in VA
491 was higher than in GE, thus may have been less prone to resurface buried cells by
492 vertical mixing (Delgado et al., 1991). However, the higher k_C values observed for GE
493 samples, representing a steeper vertical variation in Chl *a*, is indicative of a lower
494 degree of vertical mixing. When exposed to photosynthesis-promoting conditions,
495 buried MPB cells recovered PSII activity in a relatively short period (3 h), but only to a
496 fraction of the ΦPSII values observed at the surface. It may be hypothesized that the
497 recovery of the photosynthetic activity occurs in a two-step process: the described fast

induction leading to intermediate, depth-dependent ΦPSII levels, being followed by a longer acclimation process leading to the full recovery of ΦPSII to values comparable to those at the surface.

Viable cells were found at depths considerably larger (cm-scale) than the depth of the photic zone or its vicinity (sub-millimeter scale). Together with the ability to regain PSII functionality within 3h, demonstrates its ecological relevant. This buried fraction of MPB biomass allows to act as a reservoir for replacing cells at the surface which may be suddenly removed by resuspension or grazing. This could attenuate fluctuations in the productive biomass formed by microalgal cells present in the photic zone. This in turn may contribute to increase the resilience of MPB communities in face of external perturbations, and to reinforce the role of MPB as source of cells for phytoplankton (Barnett et al., 2015; Guarini et al., 2004; Lewis et al., 1999).

This functional resilience requires that benthic diatoms (i) can survive for long periods in darkness and in anoxia and (ii) maintain the capacity to promptly resume photosynthetic activity. There is solid experimental evidence that some diatoms can survive long periods of darkness (Antia and Cheng, 1970; Itakura et al., 1997; Murphy and Cowles, 1997; Peters and Thomas, 1996; Reeves et al., 2011; Smayda and Mitchell-Innes, 1974). Already in the 1970s (Antia and Cheng, 1970) it was found that *Phaeodactylum tricornutum* was able to survive up to six months in the dark, with a few individuals surviving up to 17 months. Subsequent studies have confirmed that planktonic centric diatoms species were also capable of withstanding long dark periods. *Thalassiosira antarctica*, *T. tunida* and *Proboscis inermis* were shown to survive from four to nine months in the dark, maintaining high levels of photosynthesis during the first three months (Peters and Thomas, 1996),

Survival in darkness or while buried is supported by the formation of morphological unchanged resting cells (Jewson et al., 2006; McQuoid and Hobson, 1996), or sporulation (Sugie and Kuma, 2008). The latter was shown by both laboratory (Durbin, 1978; Jochem, 1999; Lewis et al., 1999) and field studies, using diatoms from deep sea (Cahoon et al., 1995; Wasmund, 1989), Antarctic sediments (Wulff, 2008), or the alteration of the gene expression level of the LHCs family as described by Nymark et al., (2013). Diatoms thus have the capacity to live heterotrophically, enabling survival based on organic energy sources (Kamp et al., 2011; Lewin, 1953; McMinn and Martin, 2013; Schaub et al., 2017; Tuchman et al., 2006). Facultative heterotrophy of diatoms is a long-known mechanism enabling survival in the absence of light (Lewin, 1953). Although it seems more common among pennate, benthic forms (Lewin and Hellebust, 1970; Rivkin and Putt, 1987), it was shown to also occur in centric diatoms (Kamp et al., 2013; White, 1974). Peters, (1996) suggested a re-utilization of organics derived from senescent members of the population, which is a plausible scenario in the case of buried MPB populations.

The reactivation of photosynthetic activity of diatoms after prolonged dark periods has also been shown to occur in a variety of conditions and for different species. The pennate species *P. tricornutum* and several other diatom species are able to resume growth in light after 24 to 68 weeks in the dark (Antia and Cheng, 1970), and ice diatoms are able to resume photosynthetic activity after 64 days in darkness (Wulff et al., 2008). The fast recovery of photosynthetic activity seems to be based on the ability of diatoms to maintain a functional photosynthetic apparatus during dark periods (Nymark et al., 2013), supported by a very slow degradation of photosynthetic pigments during long periods of darkness and anoxia (Jewson et al., 2006; Kamp et al., 2013; Larson and Sundbäck, 2012; Wasmund, 1989).

The significance of buried MPB regaining its photosynthetic activity presented in this study nevertheless is limited in two main ways: first, they do not provide any indication on how long the cells had been buried before being exposed to light and air. This makes it difficult to compare the results with ones performed under controlled laboratory conditions (e.g. known time of darkness), or to relate the rates of vertical decrease of Chl *a* with temporal processes. A second limitation regards the fact that the techniques used cannot determine the fraction of buried cells that remain viable, as chlorophyll fluorescence indices like ΦPSII are largely independent of the absolute number of photosynthetic cells. Therefore, it will only detect signals emitted from functional cells, even if present in small numbers (Franklin et al., 2009).

4.2. Subsurface vertical migration

Vertical migration by benthic pennate diatoms in tidal sediments has been extensively studied (Coelho et al., 2011; Consalvey et al., 2004; Easley et al., 2005; Herlory et al., 2004; Janssen et al., 1999; Round, 1979; Underwood et al., 2005). The migratory behavior of pennate diatoms is partially controlled by endogenous rhythms, responsible for triggering movement in the absence of external stimuli (Coelho et al., 2011; Frankenbach et al., 2014). Most studies have been centered on the effects of vertical migration on surface MPB biomass as a main factor controlling the photosynthetic biomass in the photic zone, and thus the instantaneous rates of carbon fixation (Serôdio et al., 2001). In comparison, only a few studies have addressed the occurrence of vertical migration below the photic zone and the changes in mm-scale Chl *a* vertical profiles over time (Du et al., 2010b; Kingston, 1999; Pinckney et al., 1994).

The present work introduced the quantification of Chl a profiles with sub-millimeter vertical resolution to monitor fluxes of microalgal biomass between the

572 photic zone and subsurface layers. This technique demonstrated that subsurface vertical
573 migration can contribute to 'reinoculate' the photic zone. This is of great importance
574 after a significant disturbance (bioturbation, resuspension/deposition) causing the
575 removal of cells from the surface layers. As an increase over time of depth-integrated
576 biomass in the 0-1.0 mm depth interval was observed (Fig. 5), migration seems to occur
577 at layers deeper than those sampled. Therefore, it is possible that support that cells
578 buried down to several millimeters below the surface may reach the photic zone not
579 only passively, as via resuspension/deposition, but as well actively, due to vertical
580 migration. Although light incident at the sediment surface may had stimulated the
581 upward migration of diatoms present in the illuminated layers, endogenous behavior
582 likely played a role as well, because cells at depths of 1.0 mm may already be in the
583 dark due to the strong light attenuation in such fine sediments.

584 Earlier studies have measured vertical speeds of diatom migration between 0.17
585 and 0.28 µm s^{-1} in natural sediment (Consalvey et al., 2004). Considering that upward
586 migration may start more than four hours before the low tide and light exposure (Coelho
587 et al., 2011; Frankenbach et al., 2012), motile diatoms could cover a vertical distance of
588 about 3.2 mm along one low tide event.

589

590 *4.3. Vertical distribution of subsurface biomass*

591

592 Significant amounts of microalgal Chl *a* can be found at depths of several
593 centimeters below the sediment surface (De Jonge and Colijn, 1994; Du et al., 2010a;
594 Kingston, 1999; Sun et al., 1991). Most of these works quantified continuous cm-scale
595 vertical profiles of Chl *a* of MPB, from the surface to depths often greater than those
596 tested in the present study (10 cm) (Steele and Baird, 1968). The simple first-order

exponential model of Eq. (2) captured the main features of the vertical distribution of Chl *a* in all studied sediments (De Jonge and Colijn, 1994; Delgado et al., 1991; Du et al., 2010b; Sun et al., 1991; Weiqiu et al., 2013). The fitting of the model to experimental data was found to be significantly improved by adding a term for background biomass. This does not exclude however that this basal level (ranging from 0.88 to 4.72 µg Chl *a* g^{-1}) may not remain constant with depth and may tend to zero in deeper vertical profiles.

The estimated depth-integrated biomass decreased with increasing grain size (highest in VA and lowest in GE, intermediate values for TO), confirming earlier studies where Chl *a* profiles were compared between muddy and sandy sediments and where MPB biomass was consistently found to be higher in the former than the latter (Brotas and Serodio, 1995; Jack J. Middelburg et al., 2000). The fitting of Eq. (2), and particularly the estimation of the decay rate k_C, allows comparing the various sites regarding the shape of the vertical Chl *a* profile. Based on the estimates of the decay rate k_C and of background biomass, C_d, two different patterns emerged. Despite showing very different absolute values at the surface, samples from VA and GE showed similar vertical decay rates (1.11 and 1.26 cm^{-1}, respectively), while the value estimated for TO was substantially lower (k_C = 0.52 cm^{-1}). It is evident by comparing the ratio of surface biomass to C_d of VA and TO that sediments from TO appear to conceal more biomass below the surface. While surface biomass in VA was about twice as high as in TO, C_d values were similar (4.46 to 4.42 µg g^{-1} for VA and TO, respectively). The steepness of Chl *a* gradients is expected to decrease with mixing and increase with Chl *a* degradation (Middelburg et al., 2000; Sun et al., 1991). As such, the steeper profile observed in VA and GE may be due to lower mixing or higher pigment degradation. The observed differences may also be explained by different impacts of resuspension, as previously

622 shown (Middelburg et al., 2000; Sun et al., 1991). Considering the data available for the
623 Ria de Aveiro on sediment granulometry (Plecha et al., 2014), bathymetry (Dias et al.,
624 2003; Vargas et al., 2017), and water velocity (Lopes and Dias, 2015), the results match
625 the prediction that sediments in GE are mixed up more thoroughly than in VA.

626 Application of Eq. (2) also evaluated the fraction of subsurface Chl *a*, to our
627 knowledge not done in previous studies which characterized cm-scale vertical profiles
628 of Chl *a* in estuarine or marine sediments (Du and Chung, 2009; Weiqiu et al., 2013).
629 The proportion of MPB biomass below the surface layers was found to reach substantial
630 values, as indicated by the large $C_{sub,total}$ values that were estimated, which ranged from
631 close to 3 (GE) to values around 5 (VA and TO). These values may, however, be
632 considered conservative estimates, since they are based on relatively short vertical
633 profiles (0-6 cm deep, when Chl *a* has been reported to be found at deeper layers), and
634 because 'surface' biomass was considered the top 5 mm depth interval, a depth range
635 clearly much larger than the actual photic zone, which even for the sandy site should not
636 exceed 1-2 mm.

637 Based on the results of this study, the MPB can be categorized into three
638 functional layers, i) a 'canopy', formed by the cells at the uppermost layers, which are
639 photosynthetically active, and therefore actively contributing to primary production, ii)
640 a 'cell reserve', formed by cells capable to quickly replace the ones in the surface layer
641 through vertical migration, within minutes to a few hours, and iii) a large repository of
642 cells serving as a 'backup' but also acting as a carbon sink.

643

644 *4.4. Ecosystem-level subsurface biomass and 'blue carbon' budgets*

645

The proportion of total:subsurface MPB biomass (here quantified as $C_{sub,total}$) may be used to estimate the amount of potentially productive subsurface biomass from available surface values. Traditionally, MPB 'surface' biomass has been measured by sampling the top layers of sediment, in the range 2-10 mm (Du and Chung, 2009; Kelly et al., 2001), when studies target to measure the biomass implicated in primary productivity (Laviale et al., 2015; MacIntyre and Cullen, 1995; Serôdio et al., 2001; Taylor and Paterson, 1998). More recently, optical methods such as remote sensing, based on reflectance measurements or solar-induced fluorescence became an extensively used method to estimate Chl *a* concentrations and create km-scale maps of MPB biomass and annual rates of primary production (Benyoucef et al., 2014; Bouman et al., 2017; Combe et al., 2005; Daggers et al., 2018; Huete et al., 2015; Kazemipour et al., 2012; Ryu et al., 2014; van der Wal et al., 2010). Thus, 'observable' MPB biomass is limited to the top surficial layers of sediment, missing an important fraction of standing stock of MPB biomass. Upscaling of local estimates of the fraction of Chl *a* present below the surface to the whole intertidal area of the Ria de Aveiro confirmed the relevance of the subsurface MPB biomass at the ecosystem level. In what can be a conservative estimate, the spatially-weighted average of $C_{sub,total}$ reached 3.78, indicating that more than 3/4 of the MPB biomass in the top 10 cm is sub-superficial. Considering only the potentially resilient biomass, the subsurface fraction is still substantial, with spatially-weighted $C_{sub,viable}$ reaching a value above 2.

The quantification of MPB subsurface biomass is relevant in the context of the ongoing discussion on the importance of unvegetated estuarine intertidal areas as contributors of ecosystem-level 'blue carbon' budgets (Oakes and Eyre, 2014; Oreska et al., 2018). Although the estimates in the present study were based on Chl *a* and not directly on carbon content, being therefore more closely related to the content in

671 particulate organic carbon, the produced results clearly support the idea that 'naked
672 sediments' colonized by MPB are major contributors to ecosystem-level blue carbon.
673 As more than half of the intertidal area of the Ria de Aveiro are unvegetated sediments,
674 the present results support several recent studies raising awareness for the role of these
675 areas as major sites of blue carbon location (Oakes and Eyre, 2014; Oreska et al., 2018).
676 As recognized by Wolanski et al. (2009), unvegetated estuarine areas have received
677 much less attention than vegetated areas (seagrass beds, saltmarshes, mangroves).
678 However, recent studies using ^{13}C *in situ* labeling experiments showed that most
679 sediment organic carbon is derived by MPB in both vegetated and unvegetated costal
680 habitats, and therefore contributed to the overall sediment organic contribution (Oakes
681 and Eyre, 2014; Oreska et al., 2018). Furthermore, the findings of this study also show
682 that, not only is there a significant amount of microalgal-associated carbon that is
683 'captured and hold' (configuring the 'blue carbon' paradigm), but that this biomass
684 stored in the sediments is (at least partially) photosynthetically functional, being readily
685 mobilizable to carry out additional carbon fixation. The results of this study show that
686 the large amounts of MPB biomass in sub-photic layers are likely an important
687 contributor to productive biomass, replenishing surface levels and attenuating effects of
688 local disturbances, and function not merely as primary producers but also as a major
689 carbon sink.
690

691 **Acknowledgements**

692 This work was supported by the Fundação para a Ciência e a Tecnologia (FCT), through
693 doctoral fellowship SFRH/BD/86788/2012 to S. Frankenbach and by CESAM
694 (UID/AMB/50017 – POCI-01-0145- FEDER-007638), FCT/MCTES through national
695 funds (PID- DAC), and the co-funding by the FEDER, within the PT2020 Partnership

Agreement and Compete 2020. We thank William Schmidt for revising the manuscript, and two anonymous reviewers for their critical comments.

References

Admiraal, W., 1984. The ecology of estuarine sediment-inhabiting diatoms. Prog. Phycol. Res. 3, 269–322.

Almeida, P.R., Moreira, F., Costa, J.L., Assis, C.A., Costa, M.J., 1993. The feeding strategies of Liza ramada (Risso, 1826) in fresh and brackish water in the River Tagus, Portugal. Journal of Fish Biology. J. Fish Biol. 42, 95–107. https://doi.org/10.1111/j.1095-8649.1993.tb00308

Antia, N.J., Cheng, J.Y., 1970. The survival of axenic cultures of marine planktonic algae from prolonged exposure to darkness at 20°C. Phycologia 9, 179–183. https://doi.org/http://dx.doi.org/10.2216/i0031-8884-9-2-179.1

Armbrust, E.V., 2009. The life of diatoms in the world's oceans. Nature 459, 185–92. https://doi.org/10.1038/nature08057

Barnett, A., Méléder, V., Blommaert, L., Lepetit, B., Gaudin, P., Vyverman, W., Sabbe, K., Dupuy, C., Lavaud, J., 2015. Growth form defines physiological photoprotective capacity in intertidal benthic diatoms. ISME J. 9, 32–45. https://doi.org/10.1038/ismej.2014.105

Benyoucef, I., Blandin, E., Lerouxel, A., Jesus, B., Rosa, P., Méléder, V., Launeau, P., Barillé, L., 2014. Microphytobenthos interannual variations in a north-European estuary (Loire estuary, France) detected by visible-infrared multispectral remote sensing. Estuar. Coast. Shelf Sci. 136, 43–52.

https://doi.org/10.1016/j.ecss.2013.11.007

Bondoc, K.G. V., Lembke, C., Lang, S.N., Germerodt, S., Schuster, S., Vyverman, W., Pohnert, G., 2018. Decision-making of the benthic diatom Seminavis robusta searching for inorganic nutrients and pheromones. ISME J. https://doi.org/10.1038/s41396-018-0299-2

Bouman, H.A., Platt, T., Doblin, M., Figueiras, F.G., Gudfinnsson, H.G., Huang, B., Hickman, A., Jackson, T., Lutz, V.A., Rey, F., Pepin, P., Segura, V., Tilstone, G.H., Dongen-Vogels, V. Van, 2017. Photosynthesis--irradiance parameters of phytoplankton: synthesis of a global data set marine. Earth Syst. Sci. Data Discuss. 251–266. https://doi.org/10.1594/PANGAEA.874087

Brito, A., Newton, A., Tett, P., Fernandes, T.F., 2009. Temporal and spatial variability of microphytobenthos in a shallow lagoon: Ria Formosa (Portugal). Estuar. Coast. Shelf Sci. 83, 67–76. https://doi.org/10.1016/j.ecss.2009.03.023

Brotas, V., Serodio, J., 1995. A mathematical model for the vertical distribution of Chlorophyll a in esturaine intertidal sediments. Netherlands J. Aquat. Ecol. 29, 315–321. https://doi.org/10.1007/BF02084230

Bueno-Pardo, J., García-Seoane, E., Sousa, A.I., Coelho, J.P., Morgado, M., Frankenbach, S., Ezequiel, J., Vaz, N., Quintino, V., Rodrigues, A.M., Leandro, S., Luis, A., Serôdio, J., Cunha, M.R., Calado, A.J., Lillebø, A., Rebelo, J.E., Queiroga, H., 2018. Trophic web structure and ecosystem attributes of a temperate coastal lagoon (Ria de Aveiro, Portugal). Ecol. Modell. 378, 13–25. https://doi.org/10.1016/j.ecolmodel.2018.03.009

Cahoon, L.B., 1999. The role of benthic microalgae in neritic ecosystems. Oceanogr.

743 Mar. Biol. an Annu. Rev. 37, 47–86.

744 Cahoon, L.B., Lawst, R.A., Thomas, C.J., 1995. Viable diatoms and chlorophyll a in
745 continental slope sediments off Cape Hatteras, North Carolina. Deep. Res. II 41,
746 767–782.

747 Cartaxana, P., Ruivo, M., Hubas, C., Davidson, I., Serôdio, J., Jesus, B.M., 2011.
748 Physiological versus behavioral photoprotection in intertidal epipelic and
749 epipsammic benthic diatom communities. J. Exp. Mar. Bio. Ecol. 405, 120–127.
750 https://doi.org/10.1016/j.jembe.2011.05.027

751 Coelho, H., Vieira, S., Serôdio, J., 2011. Endogenous versus environmental control of
752 vertical migration by intertidal benthic microalgae Endogenous versus
753 environmental control of vertical migration by intertidal benthic microalgae. Eur. J.
754 Phycol. Eur. J. Phycol 463, 271–281.
755 https://doi.org/10.1080/09670262.2011.598242

756 Combe, J.P., Launeau, P., Carrère, V., Despan, D., Méléder, V., Barillé, L., Sotin, C.,
757 2005. Mapping microphytobenthos biomass by non-linear inversion of visible-
758 infrared hyperspectral images. Remote Sens. Environ. 98, 371–387.
759 https://doi.org/10.1016/j.rse.2005.07.010

760 Consalvey, M., Paterson, D.M., Underwood, G.J.C., 2004. The Ups and Downs of Life
761 in a Benthic Biofilm: Migration of Benthic Diatoms. Diatom Res. 19, 181–202.
762 https://doi.org/10.1080/0269249X.2004.9705870

763 Costa, S., Picado, A., Vaz, N., Coelho, C., Portela, L., Dias, J.M., 2018. Climate
764 Change Effects on Suspended Sediment Dynamics in a Coastal Lagoon: Ria de
765 Aveiro (Portugal). J. Coast. Res. 85, 521–525. https://doi.org/10.2112/SI85-105.1

766 Daggers, T.D., Kromkamp, J.C., Herman, P.M.J., van der Wal, D., 2018. A model to
767 assess microphytobenthic primary production in tidal systems using satellite
768 remote sensing. Remote Sens. Environ. 211, 129–145.
769 https://doi.org/10.1016/j.rse.2018.03.037

770 De Jonge, V.N., Colijn, F., 1994. Dynamics of microphytobenthos biomass in the Ems
771 Estuary. Mar. Ecol. Prog. Ser. 104, 185–196. https://doi.org/10.3354/meps104185

772 De Jonge, V.N., van Beusekom, J.E.E., 1995. Wind□ and tide□induced resuspension of
773 sediment and microphytobenthos from tidal flats in the Ems estuary. Limnol.
774 Oceanogr. 40, 776–778. https://doi.org/10.4319/lo.1995.40.4.0776

775 Delgado, M., de Jonge, V.N., Peletier, H., 1991. Experiments on resuspension of natural
776 microphytobenthos populations. Mar. Biol. 108, 321–328.
777 https://doi.org/10.1007/BF01344347

778 Dias, J.M., Lopes, J.F., Dekeyser, I., 2003. A numerical system to study the transport
779 properties in the Ria de Aveiro lagoon. Ocean Dyn. 53, 220–231.
780 https://doi.org/10.1007/s10236-003-0048-5

781 Dias, J.M., Lopes, J.F., Dekeyser, I., 1999. Hydrological characterisation of Ria de
782 Aveiro, Portugal, in early summer. Oceanol. Acta 22, 473–485.
783 https://doi.org/10.1016/S0399-1784(00)87681-1

784 Du, G.Y., Chung, I.K., 2009. Estimating areal production of intertidal
785 microphytobenthos based on spatio-temporal community dynamics and laboratory
786 measurements. Ocean Sci. J. 44, 189–197. https://doi.org/10.1007/s12601-009-
787 0017-0

788 Du, G.Y., Oak, J.-H.H., Li, H., Chung, I.-K.K., 2010a. Effect of light and sediment

grain size on the vertical migration of benthic diatoms. Algae 25, 133–140. https://doi.org/10.4490/algae.2010.25.3.133

Du, G.Y., Son, M., An, S., Chung, I.K., 2010b. Temporal variation in the vertical distribution of microphytobenthos in intertidal flats of the Nakdong River estuary, Korea. Estuar. Coast. Shelf Sci. 86, 62–70. https://doi.org/10.1016/j.ecss.2009.10.008

Durbin, E.G., 1978. Aspects of the Biology of Resting Spores of *Thalassiosira nordenskioeldii* and *Detonula confervacea* Mar. Biol. (1978) 45: 31. https://doi.org/10.1007/BF00388975

Easley, J.T., Hymel, S.N., Plante, C.J., 2005. Temporal patterns of benthic microalgal migration on a semi-protected beach. Estuar. Coast. Shelf Sci. 64, 486–496. https://doi.org/10.1016/j.ecss.2005.03.013

Fenchel, T., Straarup, B.J., 1971. Nordic Society Oikos Vertical Distribution of Photosynthetic Pigments and the Penetration of Light in Marine Sediments Vertical distribution of photosynthetic pigments and the penetration of light in marine sediments 22, 172–182.

Field, C.B., 1998. Primary Production of the Biosphere: Integrating Terrestrial and Oceanic Components. Science (80-.). 281, 237–240. https://doi.org/10.1126/science.281.5374.237

Frankenbach, S., Pais, C., Martinez, M., Laviale, M., Ezequiel, J., Serôdio, J., 2014. Evidence for gravitactic behaviour in benthic diatoms. Eur. J. Phycol. 49, 429–435. https://doi.org/10.1080/09670262.2014.974218

Frankenbach, S., Serôdio, J., 2017. One pulse, one light curve: Fast characterization of

812 the light response of microphytobenthos biofilms using chlorophyll fluorescence.
813 Limnol. Oceanogr. Methods 15, 554–566. https://doi.org/10.1002/lom3.10180

814 Franklin, D.J., Choi, C.J., Hughes, C., Malin, G., Berges, J.A., 2009. Effect of dead
815 phytoplankton cells on the apparent efficiency of photosystem II. Mar. Ecol. Prog.
816 Ser. 382, 35–40. https://doi.org/10.3354/meps07967

817 Guarini, J.M., Gros, P., Blanchard, G., Richard, P., Fillon, A., 2004. Benthic
818 contribution to pelagic microalgal communities in two semi-enclosed, European-
819 type littoral ecosystems (Marennes-Oléron Bay and Aiguillon Bay, France). J. Sea
820 Res. 52, 241–258. https://doi.org/10.1016/j.seares.2004.04.003

821 Hagerthey, S.E., Defew, E.C., Paterson, D.M., 2002. Ulvae on Intertidal Benthic
822 Diatom Assemblages Under Different Nutrient and Temperature Regimes. Mar.
823 Ecol. Prog. Ser. 245, 47–59.

824 Herlory, O., Guarini, J.M., Richard, P., Blanchard, G.F., 2004. Microstructure of
825 microphotobenthic biofilm and its spatio temporal dynamics in an intertidal
826 mudflat (Aiguillon Bay, France). Mar Ecol Prog Ser 282, 33–44.

827 Hopkins, J.T., 1966. The role of water in the behaviour of an estuarine mud-flat diatom.
828 J. Mar. Biol. Assoc. United Kingdom 46, 617–626.
829 https://doi.org/10.1017/S0025315400033373

830 Huete, A., Ponce-campos, G.E., Zhang, Y., Restrepo-Coupe, N., Ma, X., Moran, M.S.,
831 2015. Monitoring Photosynthesis from Space. pp. 3–22.

832 Itakura, S., Imai, I., Itoh, K., 1997. “Seed bank” of coastal planktonic diatoms in bottom
833 sediments of Hiroshima Bay, Seto Inland Sea, Japan. Mar. Biol. 128, 497–508.
834 https://doi.org/10.1007/s002270050116

835 Janssen, M., Hust, M., Rhiel, E., Krumbein, W.E., 1999. Vertical migration behaviour
836 of diatom assemblages of Wadden Sea sediments (Dangast, Germany): A study
837 using cryo-scanning electron microscopy. Int. Microbiol. 2, 103–110.

838 Jewson, D.H., Lowry, S.F., Bowen, R., 2006. Co-existence and survival of diatoms on
839 sand grains. Eur. J. Phycol. 41, 131–146.
840 https://doi.org/10.1080/09670260600652903

841 Jochem, F.J., 1999. Dark survival strategies in marine phytoplankton assessed by
842 cytometric measurement of metabolic activity with fluorescein diacetate. Mar.
843 Biol. 135, 721–728. https://doi.org/10.1007/s002270050673

844 Kamp, A., de Beer, D., Nitsch, J.L., Lavik, G., Stief, P., 2011. Diatoms respire nitrate to
845 survive dark and anoxic conditions. Proc. Natl. Acad. Sci. 108, 5649–5654.
846 https://doi.org/10.1073/pnas.1015744108

847 Kamp, A., Stief, P., Knappe, J., De Beer, D., 2013. Response of the ubiquitous pelagic
848 diatom Thalassiosira weissflogii to darkness and anoxia. PLoS One 8, 1–11.
849 https://doi.org/10.1371/journal.pone.0082605

850 Kazemipour, F., Launeau, P., Méléder, V., 2012. Microphytobenthos biomass mapping
851 using the optical model of diatom biofilms: Application to hyperspectral images of
852 Bourgneuf Bay. Remote Sens. Environ. 127, 1–13.
853 https://doi.org/10.1016/j.rse.2012.08.016

854 Kelly, J.A., Honeywill, C., Paterson, D.M., 2001. Microscale analysis of chlorophyll-a
855 in cohesive, intertidal sediments: the implications of microphytobenthos
856 distribution. J. Mar. Biol. Assoc. United Kingdom 81, 151–162. https://doi.org/Doi
857 10.1017/S0025315401003496

858 Kingston, M.B., 1999. Wave Effects on the Vertical Migration of Two Benthic
859 Microalgae: Hantzschia virgata var. intermedia and Euglena proxima. Estuaries 22,
860 81. https://doi.org/10.2307/1352929

861 Koh, C.-H., Khim, J.S., Araki, H., Yamanishi, H., Koga, K., 2007. Within-day and
862 seasonal patterns of microphytobenthos biomass determined by co-measurement of
863 sediment and water column chlorophylls in the intertidal mudflat of Nanaura, Saga,
864 Ariake Sea, Japan. Estuar. Coast. Shelf Sci. 72, 42–52.
865 https://doi.org/10.1016/j.ecss.2006.10.005

866 Larson, F., Sundbäck, K., 2012. Recovery of microphytobenthos and benthic functions
867 after sediment deposition. Mar. Ecol. Prog. Ser. 446, 31–44.
868 https://doi.org/10.3354/meps09488

869 Laviale, M., Ezequiel, J., Pais, C., Cartaxana, P., SerÔdio, J., 2015. The “crème brûlée”
870 sampler: A new high-resolution method for the fast vertical sampling of intertidal
871 fine sediments. J. Exp. Mar. Bio. Ecol. 468, 37–44.
872 https://doi.org/10.1016/j.jembe.2015.03.013

873 Lewin, J., Hellebust, J.A., 1970. Heterotrophic nutrition of the marine pennate diatom,
874 *Cylindrotheca fusiformis*. Can. J. Microbiol. 16, 1123–1129.
875 https://doi.org/10.1139/m70-188

876 Lewin, J.C., 1953. Heterotrophy in diatoms. J. Gen. Microbiol. 9, 305–313.
877 https://doi.org/10.1099/00221287-9-2-305

878 Lewis, J., Harris, A.S.D., Jones, K.J., Edmonds, R.L., 1999. Long-term survival of
879 marine planktonic diatoms and dinoflagellates in stored sediment samples. J.
880 Plankton Res. 21, 343–354. https://doi.org/10.1093/plankt/21.2.343

Lopes, C.L., Dias, J.M., 2015. Tidal dynamics in a changing lagoon: Flooding or not flooding the marginal regions. Estuar. Coast. Shelf Sci. 167, 14–24. https://doi.org/10.1016/j.ecss.2015.05.043

Lorenzen, C.J., 1967. Determination of Chlorophyll and Pheo-Pigments: Spectrophotometric Equations. Limnol. Oceanogr. 12, 343–346. https://doi.org/10.4319/lo.1967.12.2.0343

MacIntyre, H.L., Cullen, J.J., 1995. Fine-scale vertical resolution of chlorophyll and photosynthetic parameters in shallow-water benthos. Mar. Ecol. Prog. Ser. 122, 227–238. https://doi.org/Doi 10.3354/Meps122227

McLachlan, D.H., Brownlee, C., Taylor, A.R., Geider, R.J., Underwood, G.J.C., 2009. Light-induced motile responses of the estuarine benthic diatoms Navicula perminuta and Cylindrotheca closterium (bacillariophyceae). J. Phycol. 45, 592–599. https://doi.org/10.1111/j.1529-8817.2009.00681.x

McMinn, A., Martin, A., 2013. Dark survival in a warming world. Proc. R. Soc. Biol. Sci. 280, 20122909. https://doi.org/10.1098/rspb.2012.2909

McQuoid, M.R., Hobson, L.A., 1996. Diatom resting stages. J. Phycol. 32, 889–902. https://doi.org/10.1111/j.0022-3646.1996.00889.x

Middelburg, J.J., Barranguet, C., Boschker, H.T.S., Herman, P.M.J., Moens, T., Heip, C.H.R., 2000. The fate of intertidal microphytobenthos carbon: An in situ 13C-labeling study. Limnol. Oceanogr. 45, 1224–1234. https://doi.org/10.4319/lo.2000.45.6.1224

Moerdijk-Poortvliet, T.C.W., van Breugel, P., Sabbe, K., Beauchard, O., Stal, L.J., Boschker, H.T.S., 2018. Seasonal changes in the biochemical fate of carbon fixed

by benthic diatoms in intertidal sediments. Limnol. Oceanogr. 63, 550–569. https://doi.org/10.1002/lno.10648

Mundree, S., Perissinotto, R., Nozais, C., 2003. Seasonal variations in the vertical distribution of benthic microalgae in the upper sediment of the Mdloti Estuary, South Africa. Bot. Mar. 46, 323–331. https://doi.org/10.1515/BOT.2003.029

Murphy, A.M., Cowles, T.J., 1997. Effects of darkness on multi-excitation in vivo fluorescence and survival in a marine diatom. Limnol. Oceanogr. 42, 1444–1453. https://doi.org/10.4319/lo.1997.42.6.1444

Nymark, M., Valle, K.C., Hancke, K., Winge, P., Andresen, K., Johnsen, G., Bones, A.M., Brembu, T., 2013. Molecular and Photosynthetic Responses to Prolonged Darkness and Subsequent Acclimation to Re-Illumination in the Diatom Phaeodactylum tricornutum. PLoS One 8. https://doi.org/10.1371/journal.pone.0058722

Oakes, J.M., Eyre, B.D., 2014. Transformation and fate of microphytobenthos carbon in subtropical, intertidal sediments: Potential for long-term carbon retention revealed by 13C-labeling. Biogeosciences 11, 1927–1940. https://doi.org/10.5194/bg-11-1927-2014

Oreska, M.P.J.J., Wilkinson, G.M., McGlathery, K.J., Bost, M., Mckee, B.A., 2018. Non-seagrass carbon contributions to seagrass sediment blue carbon. Limnol. Oceanogr. 63, S3–S18. https://doi.org/10.1002/lno.10718

Perkins, R.G., Lavaud, J., Serôdio, J., Mouget, J.L., Cartaxana, P., Rosa, P., Barille, L., Brotas, V., Jesus, B.M., 2010. Vertical cell movement is a primary response of intertidal benthic biofilms to increasing light dose. Mar. Ecol. Prog. Ser. 416, 93–

927 103. https://doi.org/10.3354/meps08787

928 Peters, E., 1996. Prolonged darkness and diatom mortality:II. Marine temperate species.
929 J. Exp. Mar. Bio. Ecol. 207, 43–58. https://doi.org/10.1016/S0022-0981(96)02520-
930 8

931 Peters, E., Thomas, D.N., 1996. Prolonged darkness and diatom mortality I: Marine
932 antarctic species. J. Exp. Mar. Bio. Ecol. 207, 25–41.
933 https://doi.org/10.1016/S0022-0981(96)02520-8

934 Pinckney, J., Piceno, Y., Love, C.R., 1994. Short-Term Changes in the Vertical
935 Distribution of Benthic Microalgal Biomass 9, 143–153.

936 Pinckney, J.L., Zingmark, R.G., 1993. Modeling the Annual Production of Intertidal
937 Benthic Microalgae in Estuarine Ecosystems. J. Phycol. 29, 396–407.
938 https://doi.org/10.1111/j.1529-8817.1993.tb00140.x

939 Plecha, S., Picado, A., Chambel-Leitão, P., Dias, J.M., Vaz, N., 2014. Study of
940 suspended sediment dynamics in a temperate coastal lagoon: Ria de Aveiro
941 (Portugal). J. Coast. Res. 70, 604–609. https://doi.org/10.2112/SI70-102.1

942 Reeves, S., McMinn, A., Martin, A., 2011. The effect of prolonged darkness on the
943 growth, recovery and survival of Antarctic sea ice diatoms. Polar Biol. 34, 1019–
944 1032. https://doi.org/10.1007/s00300-011-0961-x

945 Rivkin, R.B., Putt, M., 1987. Diel periodicity of photosynthesis in polar phytoplankton:
946 Influence on primary production. Science (80-.). 238, 1285–1288.
947 https://doi.org/10.1126/science.238.4831.1285

948 Round, F.E., 1979. A diatom assemblage living below the surface of intertidal sand

949 flats. Mar. Biol. 54, 219–223. https://doi.org/10.1007/BF00395784

950 Round, F.E., Palmer, J.D., 1966. Persistent, vertical-migration rhythms in benthic
951 microflora.: II. Field and laboratory studies on diatoms from the banks of the river
952 avon. J. Mar. Biol. Assoc. United Kingdom 46, 191–214.
953 https://doi.org/10.1017/S0025315400017641

954 Ryu, J.H., Choi, J.K., Lee, Y.K., 2014. Potential of remote sensing in management of
955 tidal flats: A case study of thematic mapping in the Korean tidal flats. Ocean
956 Coast. Manag. 102, 458–470. https://doi.org/10.1016/j.ocecoaman.2014.03.003

957 Sarthou, G., Timmermans, K.R., Blain, S., Tréguer, P., 2005. Growth physiology and
958 fate of diatoms in the ocean: A review. J. Sea Res. 53, 25–42.
959 https://doi.org/10.1016/j.seares.2004.01.007

960 Schaub, I., Wagner, H., Graeve, M., Karsten, U., 2017. Effects of prolonged darkness
961 and temperature on the lipid metabolism in the benthic diatom Navicula perminuta
962 from the Arctic Adventfjorden, Svalbard. Polar Biol. 40, 1425–1439.
963 https://doi.org/10.1007/s00300-016-2067-y

964 Serôdio, J., 2004. Analysis of variable chlorophyll fluorescence in microphytobenthos
965 assemblages: Implications of the use of depth-integrated measurements. Aquat.
966 Microb. Ecol. 36, 137–152. https://doi.org/10.3354/ame036137

967 Serôdio, J., Coelho, H., Vieira, S., Cruz, S., 2006. Microphytobenthos vertical
968 migratory photoresponse as characterised by light-response curves of surface
969 biomass. Estuar. Coast. Shelf Sci. 68, 547–556.
970 https://doi.org/10.1016/j.ecss.2006.03.005

971 Serôdio, J., Da Silva, J.M., Catarino, F., 2001. Use of in vivo chlorophyll a fluorescence

to quantify short-term variations in the productive biomass of intertidal microphytobenthos. Mar. Ecol. Prog. Ser. 218, 45–61. https://doi.org/10.3354/meps218045

Serôdio, J., Marques da Silva, J., Catarino, F., 1997. Nondestructive tracing of migratory rhythms of intertidal benthic microalgae using in vivo chlorophyll a fluorescence. J. Phycol 33, 542–553.

Serôdio, J., Silva, R., Ezequiel, J., Calado, R., 2011. Photobiology of the symbiotic acoel flatworm Symsagittifera roscoffensis: Algal symbiont photoacclimation and host photobehaviour. J. Mar. Biol. Assoc. United Kingdom 91, 163–171. https://doi.org/10.1039/c4dt01108b

Serôdio, J., Vieira, S.S., Barroso, F., 2007. Relationship of variable chlorophyll fluorescence indices to photosynthetic rates in microphytobenthos. Aquat. Microb. Ecol. 49, 71–85. https://doi.org/10.3354/ame01129

Smayda, T.J., Mitchell-Innes, B., 1974. Dark survival of autotrophic, planktonic marine diatoms. Mar. Biol. 25, 195–202. https://doi.org/10.1007/BF00394965

Stanley, R.H.R., Howard, E.M., 2013. Quantifying photosynthetic rates of microphytobenthos using the triple isotope composition of dissolved oxygen. Limnol. Oceanogr. Methods 11, 360–373. https://doi.org/10.4319/lom.2013.11.360

Steele, J.H., Baird, I.E., 1968. Production ecology of a sandy beach. Limnol. Oceanogr. 14–25.

Sugie, K., Kuma, K., 2008. Resting spore formation in the marine diatom Thalassiosira nordenskioeldii under iron- and nitrogen-limited conditions. J. Plankton Res. 30, 1245–1255. https://doi.org/10.1093/plankt/fbn080

995 Sun, M., Aller, R.C., Lee, C., 1991. Early diagenesis of chlorophyll-a in Long Island
996 Sound sediments: A measure of carbon flux and particle reworking. J. Mar. Res.
997 49, 379–401. https://doi.org/10.1357/002224091784995927

998 Taylor, I.S., Paterson, D.M., 1998. Microspatial variation in carbohydrate
999 concentrations with depth in the upper millimetres of intertidal cohesive sediments.
1000 Estuar. Coast. Shelf Sci. 46, 359–370. https://doi.org/10.1006/ecss.1997.0288

1001 Tomás, L.M., Rodrigues, M., Fortunato, A.B., Azevedo, A., Leitão, P.C., Oliveira, A.,
1002 Rocha, A., Lopes, J.F., Dias, J.M., 2014. Salinity modelling accuracy of a coastal
1003 lagoon: a comparative river flow analysis of basin model vs. traditional
1004 approaches. J. Coast. Res. 70, 586–591. https://doi.org/10.2112/SI70-099.1

1005 Tréguer, P., Bowler, C., Moriceau, B., Dutkiewicz, S., Gehlen, M., Aumont, O., Bittner,
1006 L., Dugdale, R., Finkel, Z., Iudicone, D., Jahn, O., Guidi, L., Lasbleiz, M.,
1007 Leblanc, K., Levy, M., Pondaven, P., 2018. Influence of diatom diversity on the
1008 ocean biological carbon pump. Nat. Geosci. 11, 27–37.
1009 https://doi.org/10.1038/s41561-017-0028-x

1010 Tuchman, N.C., Schollett, M.A., Rier, S.T., Geddes, P., 2006. Differential heterotrophic
1011 utilization of organic compounds by diatoms and bacteria under light and dark
1012 conditions. Hydrobiologia 561, 167–177. https://doi.org/10.1007/s10750-005-
1013 1612-4

1014 Ubertini, M., Lefebvre, S., Rakotomalala, C., Orvain, F., 2015. Impact of sediment
1015 grain-size and biofilm age on epipelic microphytobenthos resuspension. J. Exp.
1016 Mar. Bio. Ecol. 467, 52–64. https://doi.org/10.1016/j.jembe.2015.02.007

1017 Underwood, G.J.C., Kromkamp, J., 1999. Primary production by phytoplankton and

microphytobenthos in estuaries. Adv. Ecol. Res. 29, 93–153. https://doi.org/10.1016/S0065-2504(08)60192-0

Underwood, G.J.C., Perkins, R.G., Consalvey, M.C., Hanlon, A.R.M., Oxborough, K., Baker, N.R., Paterson, D.M., 2005. Patterns in microphytobenthic primary productivity : Species-specific variation in migratory rhythms and photosynthetic efficiency in mixed-species biofilms. Limnol. Oceanogr. 50, 755–767. https://doi.org/10.4319/lo.2005.50.3.0755

van der Wal, D., Wielemaker-van den Dool, A., Herman, P.M.J., 2010. Spatial synchrony in intertidal benthic algal biomass in temperate coastal and estuarine ecosystems. Ecosystems 13, 338–351. https://doi.org/10.1007/s10021-010-9322-9

Vargas, C.I.C., Vaz, N., Dias, J.M., 2017. An evaluation of climate change effects in estuarine salinity patterns: Application to Ria de Aveiro shallow water system. Estuar. Coast. Shelf Sci. 189, 33–45. https://doi.org/10.1016/j.ecss.2017.03.001

Wasmund, N., 1989. Micro-autoradiographic determination of the viability of algae inhabiting deep sediment layers. Estuar. Coast. Shelf Sci. 28, 651–656. https://doi.org/10.1016/0272-7714(89)90052-8

Weiqiu, L., Jielong, Z., Guanghong, T., Hualin, X., Xiaohua, Y., 2013. Temporal and vertical distribution of microphytobenthos biomass in mangrove sediments of Zhujiang (Pearl River) Estuary. Acta Oceanol. Sin. 32, 82–88. https://doi.org/10.1007/s13131-013-0302-8

White, W.A., 1974. Uptake of organic compounds by two facultatively heterotrophic marine centric diatoms. J. Phycol. 433–438.

Wolanski, E., Brinson, M.M., Cahoon, D.R., Perillo, G.M.E., 2009. Coastal Wetlands:

1041 A Synthesis. Coastal Wetlands: An Integrated Ecosystem Approach 2-38

1042 Wulff, A., Roleda, M.Y., Zacher, K., Wiencke, C., 2008. Exposure To Sudden Light

1043 Burst After Prolonged Darkness—a Case Study on Benthic Diatoms in Antarctica.

1044 Diatom Res. 23, 519–532. https://doi.org/10.1080/0269249X.2008.9705774